



City Research Online

City, University of London Institutional Repository

Citation: Xiong, Z., Guan, C., Duan, Z., Cheng, T., Ye, P., Yang, J., Shi, J., Yang, J., Yuan, L. & Grattan, K. T. V. (2022). All-optical vector magnetic field sensor based on a side-polished two-core fiber Michelson interferometer. *Optics Express*, 30(13), pp. 22746-22754. doi: 10.1364/oe.460692

This is the published version of the paper.

This version of the publication may differ from the final published version.

Permanent repository link: <https://openaccess.city.ac.uk/id/eprint/28377/>

Link to published version: <https://doi.org/10.1364/oe.460692>

Copyright: City Research Online aims to make research outputs of City, University of London available to a wider audience. Copyright and Moral Rights remain with the author(s) and/or copyright holders. URLs from City Research Online may be freely distributed and linked to.

Reuse: Copies of full items can be used for personal research or study, educational, or not-for-profit purposes without prior permission or charge. Provided that the authors, title and full bibliographic details are credited, a hyperlink and/or URL is given for the original metadata page and the content is not changed in any way.

City Research Online:

<http://openaccess.city.ac.uk/>

publications@city.ac.uk



All-optical vector magnetic field sensor based on a side-polished two-core fiber Michelson interferometer

ZIYANG XIONG,¹ CHUNYING GUAN,^{1,*} ZHENYU DUAN,¹ TAILEI CHENG,¹ PENG YE,¹ JING YANG,¹ JINHUI SHI,¹  JUN YANG,¹ LIBO YUAN,¹  AND K. T. V. GRATTAN² 

¹Key Laboratory of In-Fiber Integrated Optics of Ministry of Education, College of Physics and Optoelectronic Engineering, Harbin Engineering University, Harbin 150001, China

²School of Mathematics, Computer Science and Engineering, City, University of London, Northampton Square, London, EC1V 0HB, UK

*cyguan@163.com

Abstract: A magnetic field sensor based on a side-polished two-core fiber (SPTCF)-based Michelson interferometer (MI) has been developed and demonstrated. The magnetic field sensor is composed of a standard single mode fiber (SMF) and a section of tapered TCF. By side-polishing a segment of the TCF, the effective index of the exposed core can be made sensitive to the environmental refractive index (RI). To evaluate its performance, a magnetic fluid is used to cover the polished region with a magnetic field sensitive material, where the sensor then measures the magnetic field intensity by sensing the RI change of the magnetic fluid through the evanescent field in the polished core. The SPTCF MI device developed allows for vector magnetic field sensing because of its asymmetric structure, with its highest directional sensitivity being 55.2 pm/degree. Experimental results obtained show that when the magnetic field is parallel to the side-polished plane, a sensitivity of 1.262 nm/mT can be achieved, operating over the magnetic flux density region of 0-5 mT and over a temperature range of 20~85 °C, where the device is minimally affected by temperature changes. The sensor is well suited to a variety of potential applications given its low cost, strong anti-interference ability, simple structure and high stability.

© 2022 Optica Publishing Group under the terms of the [Optica Open Access Publishing Agreement](#)

1. Introduction

Compared with traditional electromagnetic sensors, optical fiber magnetic field sensors have attracted widespread attention due to their high sensitivity, compact size and low susceptibility to interference. A magnetic fluid (MF) is a kind of stable colloidal system consisting of 10 nm magnetic nanoparticles coated with surfactants and dispersed in a suitable liquid carrier [1], and exhibits outstanding magneto-optic properties in the external magnetic field, including tunable transmission loss [2], dichroism effects [3], birefringence effect [4,5] and tunable (refractive index) RI [6–8]. When there is no external magnetic field present, the magnetic nanoparticles are randomly and uniformly distributed around the fiber. Under the influence of the magnetic field, the nanoparticles will change from their original random state to a chain arrangement, and the RI of the MF changes accordingly. In the last decade, many different optical devices based on the MFs have been designed to allow for applications in various fields, such as magnetic resonance imaging [9], current sensing [10] and oxygen sensing [11]. Various structural fibers integrated with magnetic materials have been proposed to optimize the performance of the sensors, for example photonic crystal fibers (PCFs) [12], microfibers [13], gratings [14,15], D-shaped fibers [16] and interferometers [17]. In 2012, a magnetic field sensor based on the SMF-PCF-SMF structure had been proposed [18], in which a piece of PCF filled with MF was placed between two SMFs and used for magnetic field detection, giving a sensitivity of only ~23.67 pm/mT. The

two major disadvantages in the sensor are the difficulty in injecting the MFs into the air holes of the PCF and then to splice together the SMF and PCF filled with MF. In 2014, Dong et al. [19] proposed a SMF-based Mach-Zehnder magnetic field sensor with the maximum sensitivity is 0.26 nm/mT, which was fabricated by the taper-like and lateral-offset fusion splicing technique. Miao et al. [13] have proposed a S-tapered fiber sensor with a better sensitivity of 0.56 nm/mT. It can thus be seen that reducing the diameter of the fiber is beneficial to improve the sensitivity, but it greatly reduces the mechanical strength of the fiber, resulting in poor sensor robustness.

The sensors discussed above have mainly been used to detect the scalar magnetic field strength while measurements of magnetic field orientation are rarely reported. In 2020, Chen et al. [20] proposed a magnetic field sensor constructed by depositing a gold film on side-polished multimode fiber, in which and the surface plasmon resonance was generated to measure magnetic field direction and a sensitivity of 0.53 nm/mT was obtained. Although this magnetic vector sensor has a high sensitivity, it cannot be widely used due to high cost of the noble metals required for its construction.

In this work, an all-fiber magnetic field sensor based on a side-polished two-core fiber (SPTCF) Michelson interferometer (MI) has been demonstrated. The unpolished core of TCF is not affected by the MF and serves as a reference arm, while the side-polished core directly interacts with the MF as a sensing arm. If an external magnetic field is present, the RI of the MF in the polished region changes with the intensity and vector direction of the magnetic field. The change of the effective RI difference between the two cores causes the shift of peak wavelength of the MI creating a sensor which is capable of simultaneously sensing the magnetic field strength and orientation.

2. Structure and principle of optical fiber sensor

The cross section of the TCF used is shown in Fig. 1(a). The two cores are identical, of diameter 9 μm . They are symmetrically distributed in the cladding with a diameter of 123 μm and the distance between the two cores centers is 64 μm . The refractive index, n_1 , of the core and the refractive index difference between the core and cladding are 1.448 and 0.0042, respectively. The configuration of the proposed fiber sensor is shown in Fig. 1(b). To improve the sensitivity of the sensor, the TCF should have a strong evanescent field, and therefore one core of the TCF has been polished and exposed to the air (by using side-wheel polishing technology). The polished area is used as the sensing arm of the interferometer, allowing the polished core to interact directly with the MF to achieve a high sensitivity. The polishing depth of the TCF is defined as d , as illustrated in Fig. 1(c). The cross section of the SPTCF is shown in Fig. 1(d), where one core was polished. The polished core of TCF was connected to the core of the SMF, carefully without misalignment by using a commercial fiber splicer in manual mode, to prevent the excitation of cladding mode. Then, a coupler was formed by tapering the TCF near the fusion point, as shown in Fig. 1(b). As the fiber becomes thinner and light in the polished core is coupled into the unpolished core, two reflected beams, from the silica-air interface at the other end of the TCF, are recoupled in the tapered region and form a MI. The reflected light was monitored in real time using an Optical Spectral Analyzer (OSA) (YOKAGAWA, AQ6370C). The extinction ratio of reflection spectrum first increased and then decreased with decreasing the fiber diameter. The extinction ratio obtains its maximum when the light energy of the two cores is approximately equal. Therefore, when the interference spectrum observed on the OSA reaches its maximum extinction ratio, the tapering process was stopped immediately.

The magnetic field sensor system designed in this work is shown in Fig. 2. The system design comprises a super-continuum laser (NKT Superk COMPACT), an OSA, a fiber circulator, an electromagnet and a side-polished TCF MI immersed in the MF. The light from SMF was split into the two cores, respectively, of the TCF in the tapered zone. Light propagation in the polished core was affected by the surrounding MF and when the electromagnet supplies a magnetic field

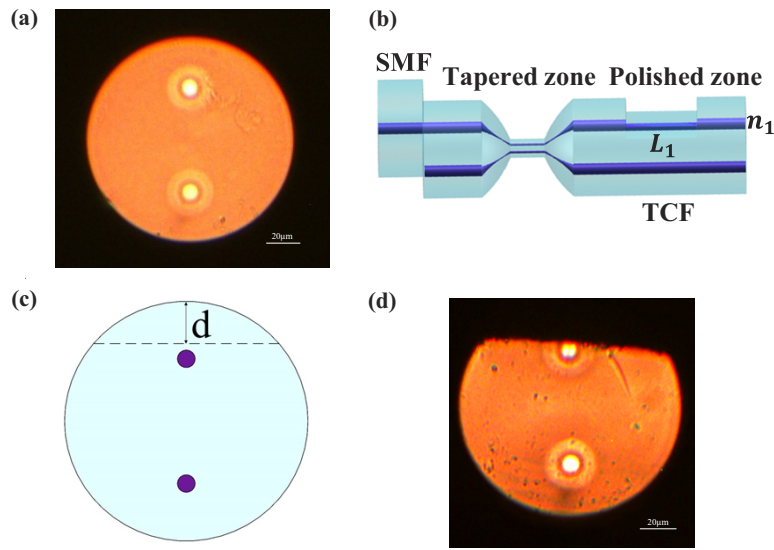


Fig. 1. (a) Cross section of the TCF. (b) 3D schematic of the magnetic field sensor. (c) Schematic diagram and (d) cross section of the polished TCF.

(with different strengths in the calibration), the change in the refractive index of the MF causes a phase shift in the polished core, compared with the unpolished core. The OSA was used to monitor the reflection spectrum. To obtain a stable optical path difference and a relatively ideal free spectral range, the TCF are bent to some extent.

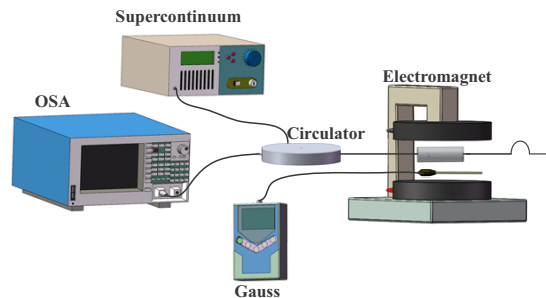


Fig. 2. Schematic diagram of magnetic field measurement set up.

The interference intensity of MI can be expressed as

$$I = I_1 + I_2 + 2\sqrt{I_1 I_2} \cos(\Delta\varphi) \quad (1)$$

$$\Delta\varphi(x) = \frac{4\pi\Delta n L_1}{\lambda} + \frac{4\pi n_1 \Delta L}{\lambda} \quad (2)$$

where I_1 and I_2 are the light intensities in the polished core and the unpolished core of the TCF, respectively. $\Delta\varphi$ is the phase difference which is mainly influenced by effective refractive index difference, Δn , between the two cores in the polished area. Further, L_1 is the polished length, ΔL is the length difference between the two cores due to the bending. Therefore, using this set up, it is possible to measure the intensity of the external magnetic field indirectly by identifying the drift of the interference peak.

3. Experimental results and discussions

The polished length of sample I is 8 mm, and the side polishing depth $d = 29.5 \mu\text{m}$; that is, half of the fiber core was polished away. The loss is $\sim 12 \text{ dB}$, introduced by the polishing process. Sample I was put into the capillary; thus its polished surface was kept straight. The glycerin solutions used, which had refractive indexes varying from 1.396 to 1.408, were injected into the capillary with a syringe, in turn. After the solution was injected, the spectrum was recorded when the spectrum was seen to be stable. The sensor reflection spectra, obtained with different refractive index matching solutions, are shown in Fig. 3(a). With the increase of the refractive index, the reflection spectrum has shown a blue shift. The direction of the spectral shift depends on the bending direction of the TCF. When the bending direction is toward the polished core, the polished core is compressed and the unpolished core is stretched. When the refractive index around the polished core increases, the optical path difference between the two cores decreases further and it can be determined from Eqs. (1) and (2), so that the reflection spectrum will shift towards the shorter wavelength. Conversely, when the bending direction is toward the unpolished core, the reflection spectrum will shift towards long wavelength. The optical path difference only affects the free spectral range and has no effect on the sensitivity. The extinction ratio of the reflection spectrum is also affected, due to the change of the energy ratio between the two cores caused by the change of the evanescent field of the polishing core. There is a linear relationship between the resonance wavelength and the RI, with a sensitivity of 703.5 nm/RIU in the range of 1.396-1.408, as shown in Fig. 3(b). This indicates that the side-polished technique can produce a strong evanescent field and enhance the interaction between the fiber core and surrounding environment.

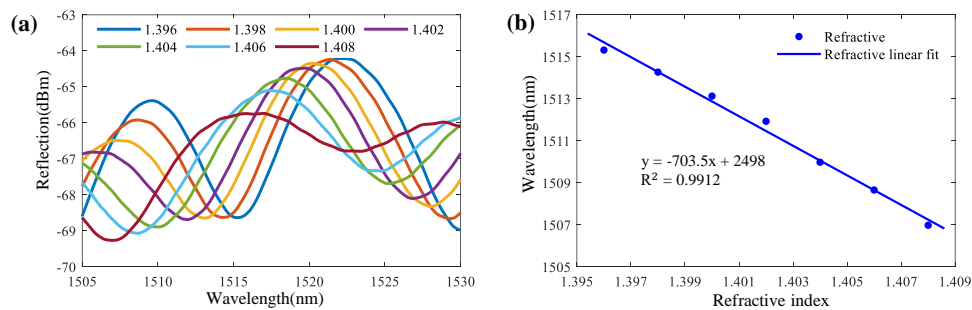


Fig. 3. (a) Reflection spectra of the SPTCF MI under different surrounding RIs and (b) resonance wavelength as a function of surrounding RI.

The process used was to rinse Sample I with deionized water, several times and then dry it, then to inject the MF (EMG605) into the capillary and seal it with AB glue, to prevent the MF from becoming volatile and leaking. After ferrofluid wrapping, the loss of the polished core is increased by about 6.5 dB. To characterize the response of the sensor to the direction of the magnetic field, a 5 mT uniform magnetic field was applied to Sample I, and the direction of the uniform magnetic field was rotated from 0° to 180° (in steps of 15°) and the reflection spectra were then recorded. Here, 0° (180°) and 90° respectively represent the two cases, where the directions of the magnetic field are parallel and perpendicular to the side polished surface. Figures 4(a) and 4(b) are the reflection spectra of Sample I to the directions of the magnetic field. When the direction of the magnetic field changes from 0° to 90° , the resonance wavelength shifts to the longer wavelength, i.e. a red shift is seen; with the direction of the magnetic field

changing from 90° to 180° , the resonance wavelength shifts to a shorter wavelength and exhibits a blue shift. Figure 4(c) shows the relationship between the resonance wavelength and the magnetic field direction. When the orientation of the magnetic field was changed from 180° to 360° , the spectra exhibit the same behavior as those seen when the shift was from 0° to 180° . To evaluate approximately the azimuthal sensitivity of the sensor, the linear fit sensitivities over the ranges from 0° - 60° and 105° - 180° were seen to be as high as 55.2 pm/deg and 35.39 pm/deg , respectively. This phenomenon can be explained by the anisotropic distribution of magnetic particles in the side-polished area. When a magnetic field was applied in a direction perpendicular to the polishing surface, the magnetic particles were evacuated from the polishing area, corresponding to the minimum RI of the MF, and the resonance wavelength becomes its maximum value. Similarly, when the direction of the magnetic field was parallel to the polishing surface, the magnetic nanoparticles converge at the side under the action of the magnetic field, corresponding to the maximum RI of the MF, and the resonance wavelength becomes a minimum. Therefore, if the direction of the magnetic field continues to change, the resonant wavelength will move back and forth between the maximum and minimum wavelengths. The sensitivity is asymmetric at the two sides of 90° . This can be interpreted as during the polishing process, the plane with the two cores is not strictly perpendicular to the polished surface and the cross section of the polished TCF was not symmetrical about 90° .

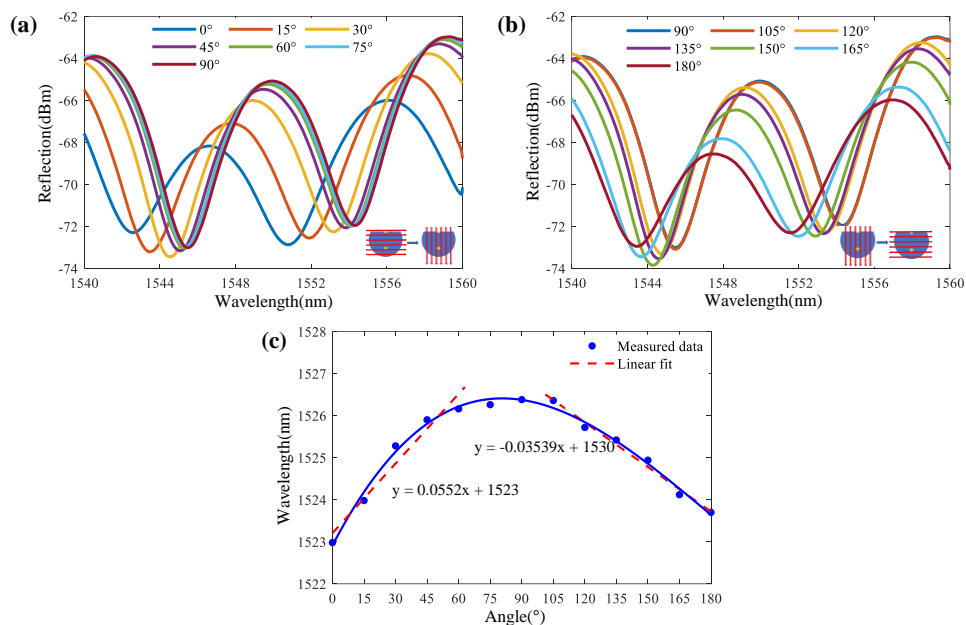


Fig. 4. Spectral responses of the sensor for different magnetic field orientations (a) 0° to 90° , (b) 90° to 180° , the applied magnetic field was fixed at 5 mT. (c) Resonant wavelength as a function of magnetic field direction

To verify the influence of magnetic field direction on the performance of magnetic field sensor, the applied magnetic fields used were both parallel and perpendicular to the polishing surface of sample I, respectively. The magnetic field strength increases gradually from 0 to 5 mT, in steps of 1 mT. Figures 5(a) and 5(b) show the reflection spectra obtained, with the variation of the magnetic field intensity. The difference between the free spectral ranges of the interference spectra for the two directions was caused by the different bending of the TCF, but this has no

effect on the sensitivity of the sensor. The shift direction of the interference spectrum depends on the distribution characteristics of the magnetic particles [21]. The magnetic field parallel to the polished surface of sample I (i.e. 0°) was first applied. Depending on the tunable refractive index of the MF, the greater the magnetic field strength, the more the magnetic particles will aggregate in the polished region to form clusters, thus the RI of the MF will increase, resulting in a blue shift of the resonance wavelength. Similarly, applying the magnetic field perpendicular to the polishing surface (that is, 90°), the more the magnetic particles will escape from the polished region when the magnetic field strength increases. Thus, the refractive index of the MF in this area will decrease, resulting in a red shift of the resonance wavelength in the reflection spectrum. A good, linear, relationship between the resonance wavelength and the magnetic field intensity in the range of 0-5 mT is shown in Fig. 5(c). The sensitivities of the sensor for the magnetic field perpendicular and parallel to the polished surface are 0.4309 nm/mT and 1.262 nm/mT, respectively. The experimental results prove that the sensitivity of the magnetic field is related to the direction of the uniform magnetic field applied.

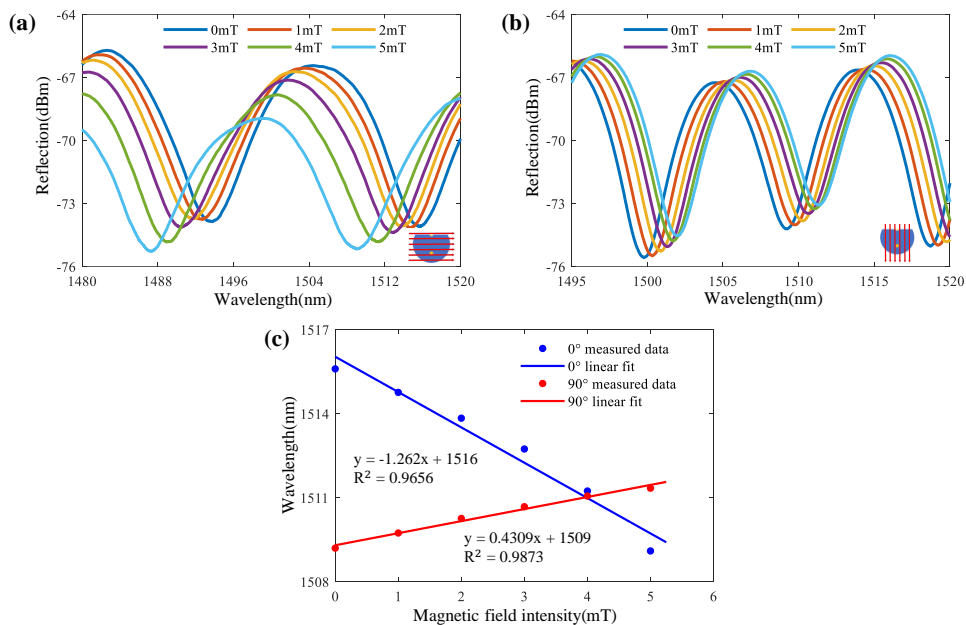


Fig. 5. Transmission spectra of the sensor for different magnetic field strengths. at (a) 0° , (b) 90° and (c) the dip wavelength as a function of magnetic field.

The side-polished depth, d , has an influence on the sensitivity of the magnetic field sensor. Samples II and III with side-polished depths of 25 μm and 20.5 μm and the same polished length of 8 mm were investigated. $d = 25 \mu\text{m}$ indicates that the side-polished plane is at a tangent to the core edge and the corresponding loss introduced by the polishing process was only 1.9 dB. A magnetic field perpendicular to the polished surface was applied to the two samples and the magnetic field strength increased from 0 to 5mT with a step of 1mT. As the magnetic field strength increases, the resonance wavelengths of two samples shifts to longer wavelengths. As shown in Fig. 6, the linear sensitivities of samples II and III are 0.108 nm/mT and 0.037 nm/mT, respectively. Comparing the sensitivities of the three samples, the greater the side-polished depth, the stronger is the evanescent field in the polished region of the TCF, the greater is the interaction between the core and the outside environment, and the greater the sensitivity of the magnetic field

sensor. However, an excessive side-throwing depth will increase the loss of the sensor, reduce the mechanical toughness of the fiber and increase the difficulty of sample preparation. Therefore, an appropriate side-polished depth should be adopted for maximum value of the sensor.

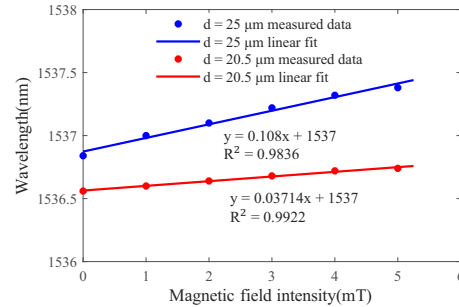


Fig. 6. Resonance wavelength of the MI as a function of magnetic field strength for different polishing depths $d = 25$ and $20.5 \mu\text{m}$.

Temperature is an important factor that affects the measurement accuracy of the magnetic field sensor. As the temperature increases from 20°C to 85°C , the linear fitting relationship between the resonance wavelength and the temperature is as shown in Fig. 7. Over this temperature range, the sensor with the magnetic fluid has a lower temperature sensitivity of $31.53 \text{ pm}/^\circ\text{C}$, a result which has very little influence on magnetic field measurement. Therefore, the ambient temperature change has little effect on the measurement accuracy of the sensor designed, suggesting that it could readily be used in several harsh environments.

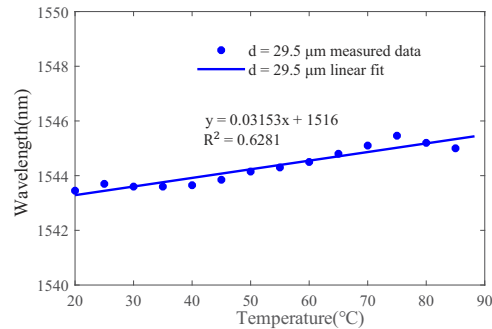


Fig. 7. The variation of resonant wavelengths of the sensor with the temperature.

For comparison, Table 1 shows the sensing structure, fabrication method, and the performance of several related magnetic field sensors discussed in the literature. It can be seen that the sensitivity of TCFMI is higher than that of the FBG magnetic field sensors reported, using magnetostrictive materials [22]. The sensors reported in the literature [13,22–24,26,27] can only measure the magnetic field strength, while the sensor developed in this work can achieve vector measurement due to its asymmetric structure. Several of the sensors reported in the literature [e.g 19, 25, 28] have been improved by using lateral offset, elliptical core fibers and bending methods to achieve moderate measurements, but these are difficult to fabricate because the amount of dislocation and bending radius are not easily controlled. The micro-structured fiber optic sensors discussed [e.g 13, 24] have higher sensitivities, but their mechanical properties and are weak and robustness limited, due to the smaller diameter. The sensor developed here has the advantages of a simple fabrication process, high sensitivity, an energy vector measurement, good mechanical

properties and robustness, all of which make it an important device for use in magnetic field monitoring and measurement.

Table 1. Sensing performance of various optical fiber magnetic field sensors.

Sensing Structure	Fabrication Method	Maximum Sensitivity	Vector-sensor	Reference
FBG	Magnetostrictive materials	0.950 pm/mT	Negative	[22]
SMS	SMF-MMF-SMF	0.905 nm/mT	Negative	[23]
Microfiber	tarped	0.56 nm/mT	Negative	[13]
Microfiber coupler	Microheater brushing technique	0.488 nm/mT	Negative	[24]
Lateral-offset TCF	Offset splicing	0.26 nm/mT	Positive	[19]
U-bent SMF	Bent	0.517 nm/mT	Positive	[25]
Asymmetric optical fiber taper	Arc discharge	0.162 nm/mT	Negative	[26]
Tapered two-mode fiber interference	Modal interference	0.982 nm/mT	Negative	[27]
Elliptical core micro fiber Bragg grating	FBG	0.081 nm/mT	Positive	[28]
TCFMI	Side polished	1.262 nm/mT	Positive	this work

4. Conclusions

In conclusion, a magnetic sensor designed using a SPTCF MI immersed in a MF has been designed and its performance discussed. The sensitivity of the refractive index of the MI (in the range of 1.396-1.408) is 703.5 nm/RIU, proving that the side-polished TCF generates a strong evanescent field. The asymmetric structure of the SPTCF allows the sensor to measure the direction of the magnetic field, and a high direction sensitivity (of 55.2 pm/degree) has been achieved. It has been found that the increase of the side-polished depth can significantly improve the sensitivity to the magnetic field. When the direction of the magnetic field was parallel to the polished surface, the highest sensitivity achieved was 1.262 nm/mT, within the magnetic field range from 0 to 5 mT, and the sensor developed as very little affected by temperature. The sensor shows the advantages of simple structure, low cost, ease of manufacture and good stability, and thus it is likely to have broad application prospects, in a range of optical devices for industrial applications.

Funding. National Natural Science Foundation of China (62105077, 62175049, U1931121); Natural Science Foundation of Heilongjiang Province (YQ2021F002, ZD2020F002); 111 project to the Harbin Engineering University(B13015).

Disclosures. The authors declare no conflicts of interest.

Data availability. Data availability. Data underlying the results presented in this paper are not publicly available at this time but may be obtained from the authors upon reasonable request.

References

1. H. T. Wang, S. L. Pu, N. Wang, S. H. Dong, and J. Huang, "Magnetic field sensing based on singlemode-multimode-singlemode fiber structures using magnetic fluids as cladding," *Opt. Lett.* **38**(19), 3765–3768 (2013).
2. J. X. Wu, Y. P. Miao, B. B. Song, W. Lin, H. Zhang, K. L. Zhang, B. Liu, and J. Q. Yao, "Low temperature sensitive intensity-interrogated magnetic field sensor based on modal interference in thin-core fiber and magnetic fluid," *Appl. Phys. Lett.* **104**(25), 252402 (2014).
3. M. Xu and P. J. Ridler, "Linear dichroism and birefringence effects in magnetic fluids," *Appl. Phys. Lett.* **82**(1), 326–332 (1997).
4. M. T. A. Elói, R. B. Azevedo, E. C. D. Lima, A. C. M. Pimenta, and P. C. Morais, "Birefringence and transmission electron microscopy of maghemite-based biocompatible magnetic fluids," *J. Magn. Magn. Mater.* **289**, 168–170 (2005).

5. Z. Y. Di, X. F. Chen, S. L. Pu, X. Hu, and Y. X. Xia, "Magnetic-field-induced birefringence and particle agglomeration in magnetic fluids," *Appl. Phys. Lett.* **89**(21), 211106 (2006).
6. S. Y. Yang, J. J. Chieh, H. E. Horng, C. Y. Hong, and H. C. Yang, "Origin and applications of magnetically tunable refractive index of magnetic fluid films," *Appl. Phys. Lett.* **84**(25), 5204–5206 (2004).
7. H. E. Horng, J. J. Chieh, Y. H. Chao, S. Y. Yang, C. Y. Hong, and H. C. Yang, "Designing optical-fiber modulators by using magnetic fluids," *Opt. Lett.* **30**(5), 543–545 (2005).
8. R. Gao, Y. Jiang, and S. Abdelaziz, "All-fiber magnetic field sensors based on magnetic fluid-filled photonic crystal fibers," *Opt. Lett.* **38**(9), 1539–1541 (2013).
9. M. L. Filograno, M. Pisco, A. Catalano, E. Forte, M. Aiello, C. Cavaliere, A. Soricelli, D. Davino, C. Visone, A. Cutolo, and A. Cusano, "Triaxial fiber optic magnetic field sensor for magnetic resonance imaging," *J. Lightwave Technol.* **35**(18), 3924–3933 (2017).
10. R. Ma, J. X. Tian, Y. J. Xia, D. G. Cao, and H. Y. Zhao, "Photo-electric hybrid current sensor combination of LPCT and FFI," *IEEE Photonics Technol. Lett.* **26**(24), 2476–2479 (2014).
11. G. Mistlberger, S. M. Borisov, and I. Klimant, "Enhancing performance in optical sensing with magnetic nanoparticles," *Sens. Actuators, B* **139**(1), 174–180 (2009).
12. Y. Chen, Q. Han, T. Liu, W. Yan, and Y. Yao, "Magnetic field sensor based on ferrofluid and photonic crystal fiber with offset fusion splicing," *IEEE Photonics Technol. Lett.* **28**(19), 2043–2046 (2016).
13. Y. P. Miao, J. X. Wu, W. Lin, K. L. Zhang, Y. J. Yuan, B. B. Song, H. Zhang, B. Liu, and J. Q. Yao, "Magnetic field tunability of optical microfiber taper integrated with ferrofluid," *Opt. Express* **21**(24), 29914–29920 (2013).
14. J. Zheng, X. Y. Dong, P. Zu, L. Y. Shao, C. C. Chan, Y. Cui, and P. P. Shum, "Magnetic field sensor using tilted fiber grating interacting with magnetic fluid," *Opt. Express* **21**(15), 17863–17868 (2013).
15. W. Lin, Y. P. Miao, H. Zhang, B. Liu, Y. G. Liu, B. B. Song, and J. X. Wu, "Two-dimensional magnetic field vector sensor based on tilted fiber Bragg grating and magnetic fluid," *J. Lightwave Technol.* **31**(15), 2599–2605 (2013).
16. L. Gao, T. Zhu, M. Deng, K. S. Chiang, X. K. Sun, X. P. Dong, and Y. S. Hou, "Long-period fiber grating within D-shaped fiber using magnetic fluid for magnetic-field detection," *IEEE Photonics J.* **4**(6), 2095–2104 (2012).
17. P. Zu, C. C. Chan, G. W. Koh, W. S. Lew, Y. X. Jin, H. F. Liew, W. C. Wong, and X. Y. Dong, "Enhancement of the sensitivity of magneto-optical fiber sensor by magnifying the birefringence of magnetic fluid film with Loyt-Sagnac interferometer," *Sens. Actuators, B* **191**, 19–23 (2014).
18. P. Zu, C. C. Chan, W. S. Lew, L. Hu, Y. X. Jin, H. F. Liew, L. H. Chen, W. C. Wong, and X. Y. Dong, "Temperature-insensitive magnetic field sensor based on nanoparticle magnetic fluid and photonic crystal fiber," *IEEE Photonics J.* **4**(2), 491–498 (2012).
19. S. H. Dong, S. L. Pu, and H. T. Wang, "Magnetic field sensing based on magnetic-fluid-clad fiber-optic structure with taper-like and lateral-offset fusion splicing," *Opt. Express* **22**(16), 19108–19116 (2014).
20. Y. F. Chen, Y. C. Hu, H. D. Cheng, F. Yan, Q. Y. Lin, Y. Chen, P. J. Wu, L. Chen, G. S. Liu, G. D. Peng, Y. H. Luo, and Z. Chen, "Side-polished single-mode-multimode-single-mode fiber structure for the vector magnetic field sensing," *J. Lightwave Technol.* **38**(20), 5837–5843 (2020).
21. Y. X. Li, S. L. Pu, Y. L. Zhao, R. Zhang, Z. X. Jia, J. L. Yao, Z. J. Hao, Z. X. Han, D. H. Li, and X. J. Li, "All-fiber-optic vector magnetic field sensor based on side-polished fiber and magnetic fluid," *Opt. Express* **27**(24), 35182–35188 (2019).
22. M. H. Yang, J. X. Dai, C. M. Zhou, and D. S. Jiang, "Optical fiber magnetic field sensors with TbDyFe magnetostrictive thin films as sensing materials," *Opt. Express* **17**(23), 20777–20782 (2009).
23. Y. F. Chen, Q. Han, T. G. Liu, X. W. Lan, and H. Xiao, "Optical fiber magnetic field sensor based on single-mode-multimode-single-mode structure and magnetic fluid," *Opt. Lett.* **38**(20), 3999–4001 (2013).
24. F. F. Wei, A. K. Mallik, D. J. Liu, Q. Wu, G. D. Peng, G. Farrell, and Y. Semenova, "Magnetic field sensor based on a combination of a microfiber coupler covered with magnetic fluid and a Sagnac loop," *Sci. Rep.* **7**(1), 1–9 (2017).
25. Y. X. Li, S. L. Pu, Z. J. Hao, S. K. Yan, Y. X. Zhang, and M. Lahoubi, "Vector magnetic field sensor based on U-bent single-mode fiber and magnetic fluid," *Opt. Express* **29**(4), 5236–5246 (2021).
26. M. Deng, D. H. Liu, and D. C. Li, "Magnetic field sensor based on asymmetric optical fiber taper and magnetic fluid," *Sens. Actuators, A* **211**, 55–59 (2014).
27. B. Sun, F. Fang, Z. Zhang, J. Xu, and L. Zhang, "High-sensitivity and low-temperature magnetic field sensor based on tapered two-mode fiber interference," *Opt. Express* **43**(6), 1311–1314 (2018).
28. R. Gao, D. F. Lu, Q. Zhang, X. Z. Xin, Q. H. Tian, F. Tian, and Y. J. Wang, "Temperature compensated three-dimension fiber optic vector magnetic field sensor based on an elliptical core micro fiber Bragg grating," *Opt. Express* **28**(5), 7721–7733 (2020).